REPORT DOCUMENTATION PAGE

Form Approved OMB No. 0704-0188

1. REPORT DATE *(DD-MM-YYYY)*	2. REPORT TYPE	3. DATES COVERED *(From – To)*
15-10-2003	Final Report	9 August 2001 - 27-Feb-04

4. TITLE AND SUBTITLE

Nonlinear microwave response of HTS microwave devices

5a. CONTRACT NUMBER
F61775-01-WE033

5b. GRANT NUMBER

5c. PROGRAM ELEMENT NUMBER

6. AUTHOR(S)

Dr. Matthias A Hein

5d. PROJECT NUMBER

5d. TASK NUMBER

5e. WORK UNIT NUMBER

7. PERFORMING ORGANIZATION NAME(S) AND ADDRESS(ES)

Universität Gesamthochschule Wuppertal
Gaußstraße 20
Wuppertal D-42097
Germany

8. PERFORMING ORGANIZATION REPORT NUMBER

N/A

9. SPONSORING/MONITORING AGENCY NAME(S) AND ADDRESS(ES)

EOARD
PSC 802 BOX 14
FPO 09499-0014

10. SPONSOR/MONITOR'S ACRONYM(S)

11. SPONSOR/MONITOR'S REPORT NUMBER(S)
SPC 01-4033

12. DISTRIBUTION/AVAILABILITY STATEMENT

Approved for public release; distribution is unlimited.

13. SUPPLEMENTARY NOTES

14. ABSTRACT

This report results from a contract tasking Universität Gesamthochschule Wuppertal as follows: The contractor will investigate the nonlinear microwave response of high-temperature superconducting films for high-performance microwave components that are used in communication, radar, and other military systems. High temperature superconducting films will be manufactured, characterized, and delivered to Lincoln Labs and AFRL/SNH (Hanscom AFB) for further evaluation.

15. SUBJECT TERMS
EOARD, Superconductivity, Microwave source, Microwave Technology

16. SECURITY CLASSIFICATION OF:			17. LIMITATION OF ABSTRACT	18. NUMBER OF PAGES	19a. NAME OF RESPONSIBLE PERSON
a. REPORT	b. ABSTRACT	c. THIS PAGE			MICHAEL KJ MILLIGAN, Lt Col, USAF
UNCLAS	UNCLAS	UNCLAS	UL	19	19b. TELEPHONE NUMBER *(Include area code)* +44 (0)20 7514 4955

IRI PROJECT REPORT #4 – FINAL REPORT

Reference Number F61775-01-WE033

Period from February 2003 until August 2003 and overview over the entire project

1. Summary of proposed research

1.1 Description of services, according to the contract

The contractor has investigated the nonlinear microwave response of high-temperature superconducting (HTS) films for high-performance microwave components that are used in communication, radar, and other systems. Contractor has provided and characterized HTS films, and delivered them to Dr. John Derov, AFRL/SNHA. Contractor's proposal "Nonlinear microwave response of HTS microwave devices", is incorporated as attachment.

1.2 Summary of research objectives, according to the proposal

The goals of the project were a comprehensive understanding and control of the nonlinear microwave response of HTS films, in terms of intermodulation distortion and power-dependent surface impedance. These goals have been achieved to a major extent, even though some puzzles related to the microscopic origin of the nonlinearities remain to be solved.

While numerous research groups and high-tech companies have demonstrated HTS devices and subsystems of unprecedented performance, the nonlinear response of the superconducting components eventually limits wider application, especially in narrowband, sharp cut-off, receive filters, or in high-power transmit filters. Among the basic features of nonlinear microwave response are a RF-current-dependent microwave surface impedance, $Z_s(I_{rf})$, and third-order two-tone frequency intermodulation distortion (IMD). Both effects have been studied for superconductors, with emphasis on HTS [1]. We have found in the course of this project that the dielectric substrates can also lead to undesirable nonlinearities, namely a RF field-dependent loss tangent, $\tan\delta(E_{rf})$, and IMD, up to temperatures close to T_c [2,3].

The microscopic origins of IMD in YBaCuO and MgO are poorly understood at present. Also, little is known about the relations between the power dissipation over microwave cycles, which is implicit in the concept of a surface impedance, and the IMD caused by two closely spaced frequency tones. Investigating and modelling the nonlinear behaviour hence challenges the development of ultra-high performance front-ends and the optimisation of new functional microwave materials [3-6].

AQ F04-09-1000

1.3 Development of the project and topical focus of the final half-year

During the course of the project, in total, 16 epitaxial YBCO films on MgO were prepared in 5 batches at QinetiQ Malvern. Additional MgO-substrates, provided by STI, LG Electronics (Seoul, Korea), Lincoln Laboratory, and eSCeTe (Cr-doped MgO), were used for Nb deposition and comparative studies. The microwave measurements were performed at LL and AFRL using the stripline resonator technique. It turned out that measurements on unpatterned films, which were intended to be established at 19 GHz [4], were not essential for the progress and success of the project. Therefore, our studies focused on the extended experimental body available from LL and AFRL. The results, analyzed and modeled by the contractor, have been published in eight papers (partly submitted to reviewed journals and partly contributed to international conferences) [2,3, 7-12]. Our results and observations attracted attention from the international scientific community and stimulated research in different places. The project has helped to identify routes to improve the power handling capability and reduce the IMD of YBCO films. Further potential benefits could result from the development of novel devices based on the nonlinear dielectric loss tangent of MgO.

During the last phase of the project, we have studied the nonlinear microwave response of a batch of overdoped YBCO films, part of which were additionally subject to Ca-doping ([7-9] and Sec. 3.1). The Ca-doping was performed by the group of Professor Jochen Mannhart at the University of Augsburg [13], whose contribution we gratefully acknowledge. The aim of this study was to find out how far the improvement of the linear microwave performance reaches into the overdoped range.

Other subjects investigated during the final half-year are the development of a phenomenological model, which relates the IMD to the nonlinear features of the kinetic conductivity of the superconductor.

2. Summary of achievements during the final half-year period

We have extended the correlations between the DC critical current density of superconducting YBCO films and their nonlinear microwave response deeper into the region of overdoped films. The RF critical current, and hence the 1-dB compression point, as well as the third-order intercept point, continue to move towards higher power for films with higher oxygen content and, possibly, ordering of the oxygen vacancies. We could not observe any indication of saturation, still leaving potential for further improvement. The carrier density can be adjusted by low-temperature anneals in activated oxygen, or by Ca-doping [13,14]. Oxygen content and ordering seem to be the key parameters to optimize the linear microwave

response of YBCO. The ordering of the oxygen vacancies is expected to be affected by adjusting the growth stoichiometry of the YBCO films, and by the annealing schedule during and after film deposition. However, reliable procedures remain to be identified.

We have developed a phenomenological model to relate the IMD signal to the nonlinear contributions of the surface impedance of superconductors. The model is based on a lumped-element equivalent circuit, which has the advantage of intuitive access. The resulting equation for the intermodulation power has been confirmed by a separate rigorous analysis of intermodulation in a distributed resonator [15], similar to the derivations in [16,17]. By comparing the IMD signal predicted by the model with our experimental data, we find the resistive nonlinearity dominating the inductive contribution to the IMD, in contrast to the theoretical expectations from [16]. Our model indicates also how data obtained for different samples or with different resonator geometries can be compared.

In addition to the superconducting nonlinearities, we have also observed that the dielectric loss tangent of MgO becomes RF field-dependent, due to resonant absorption by $Mg(OH)_2$ impurity states. The dielectric response causes marked additional microwave losses at temperatures below about 50 K. The dielectric losses include contributions from power-independent relaxation, leading to pronounced loss peaks around 25 K in the 2-GHz region. Significantly enhanced intermodulation is another consequence of the microwave loss mechanisms in MgO. Because of the high quality of our latest batch of superconducting films, we were able to observe the influence of the dielectric nonlinearities up to temperatures of about 70 K. The dielectric nonlinearites are stronger in more slowly cooled films. On the other hand, full oxygenation and good oxygen ordering require some time spent at relatively low annealing temperatures. The optimization of YBCO films on MgO for microwave device applications, therefore, requires proper adjustment of the annealing schedules during the different phases of film preparation.

Beside the relevance of our results for HTS microwave applications, our findings could affect any high-frequency application involving MgO, or similar dielectrics. The effects brought about by resonant absorption could also be used, in principle, for new types of signal detection or modulation in cryogenic dielectric microwave devices.

3. Nonlinear microwave response of YBCO

3.1 Properties of the latest batch #3318

The results achieved during the preceding phases of the project have shown that the nonlinear surface impedance (i.e., resistance and changes of the reactance) as well as the intermodulation signal decrease for increasing oxygen content [4-6]. This observation let us to prepare another batch of overdoped films, including the approach of Ca-doping, to increase the number of free charge carriers as much as possible [8,13]. Fig. 1 sketches the parameters varied in batch #5. Table I presents a complete list of the films studied in this project.

All four YBCO films of batch #5 were annealed at 540 °C in atomic oxygen after deposition (similar to the treatment of #4B). This step aimed at getting a comparable and – supposedly – homogenized distribution of oxygen vacancies. The 40-nm thick cap layers on #5A-#5C were then deposited at the University of Augsburg by pulsed laser deposition at temperatures around 750 °C. The cap layer was stoichiometric YBCO for #5A and 30%-Ca-doped YBCO for #5B and #5C. The cap layers of #5A and #5C were removed by ion milling after deposition. All films underwent a final anneal at 540 °C in atomic oxygen for 30 minutes.

According to the data in table I, all films with cap layers displayed T_c-values well below 90 K, with #5B and #5C having the lowest $T_c < 86$ K, while that of the reference film #5D remained close to 90 K. The additional deposition and corresponding annealing steps reduced the T_c-values, probably by hole doping as expected. Interestingly, though, the DC critical current densities, which still exceeded most previous J_{c60}-values, decreased, too.

Fig. 2 compares the temperature-dependent effective surface resistance of the films of batch #5 with a number of films from other batches. The most striking feature is the pronounced maximum of $R_{eff}(T)$ for batches #4 and #5. We attribute this peak to dielectric relaxation-type losses in the MgO substrate, as the slow cooling after the deposition of the YBCO base film could have favored the nucleation of $Mg(OH)_2$ precipitates [6]. Below about 20 K, the dielectric losses of MgO become dominated by resonant effects, i.e., they become power-dependent and hence nonlinear. We expect that the minimum of R_{eff} near 50 K results from the power dissipation in the superconducting film, which increases as T_c is approached.

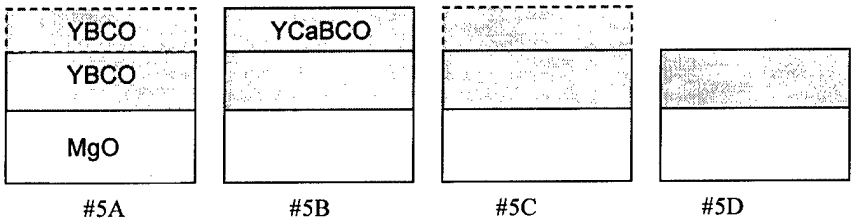

Figure 1. Schematic description of the films of batch #5 [8].

Batch/sample	T_c (K)	J_{c60} (MA/cm^2)	c-axis (nm)	oxygen. level	remarks
# 1 (2746)					
1A	89.71	12.96	---	Slightly underd.	Damaged
1B	90.45	2.67	1.1715	Near optimum	As-grown
1C	90.2	2.23	1.1716	Near optimum	Molecular O_2
1D	89.0	---	1.1703	Near optimum	Contact anneal
# 2 (2809)					
2A	91.74	11.40	1.1703	Optimal	Qualitat. data
2B	90.68	5.82	1.1725	Underdoped	Atomic oxygen
2C	84.18	10.40	1.1686	Overdoped	Atomic oxygen
2D	---	---	---	---	Damaged
# 3 (2997)					
3A	90.54	2.40	1.1734	Near optimum	As-grown
3B	92.44	6.88	1.1724	Optimal	Damaged
3C	69.3	2.67	1.1752	Underdoped	Atomic oxygen
3D	91.8	8.10	1.1702	Overdoped	Atomic oxygen
# 4 (3321)					
4A	87.75	8.38	n.m.	Overdoped	As-grown
4B	86.21	11.00	n.m.	Overdoped	Atomic oxygen *540 °C, single*
4C	86.75	9.90	n.m.	Overdoped	Atomic oxygen *400 °C, single*
4D	92.21	5.60	n.m.	Overdoped	Atomic oxygen *400°C, iterative*
# 5 (3318)					
5A	86.79	10.50	n.m.	Overdoped	YBCO cap removed
5B	82.84	12.80	n.m.	Overdoped	Ca cap
5C	85.59	12.20	n.m.	Overdoped	Ca cap removed
5D	89.40	14.60	n.m.	Overdoped	without cap layer

Table I. Updated summary of characteristic parameters of all YBCO films on MgO prepared at QinetiQ Malvern. All batches were nucleated at 680 °C, Y-rich, and grown at 700 °C, either stoichiometric (2746 and 2997), or slightly Cu-rich (2809, 3318, 3321). The T_c- and J_c-values were derived from DC magnetization measurements (further remarks see text). The oxygenation level was concluded from comparison with other samples. The cap layers used for batch 5 were 40 nm thick and consisted either of stoichiometric or 30%-Ca-doped YBCO.

Although the microwave losses in MgO and in YBCO have different temperature scales, it is illustrative to compare $R_{eff}(T)$ for batch #5 on a T-scale normalized to T_c (Fig. 3). Among batch #5, the reference film #5D displays the lowest surface resistance. The three films, which have (had) cap layers, display enhanced surface resistance at intermediate temperatures. Height and width of the dielectric loss peak vary among all four films, indicating that the nucleation of defect dipoles in MgO is strongly temperature-dependent in the range of the applied deposition temperatures, i. e., between 690 and 750 °C. The film with the Ca-rich cap on it (#5B) displays the highest surface resistance, which could result from deteriorated microwave properties in the region of high Ca-concentration [8].

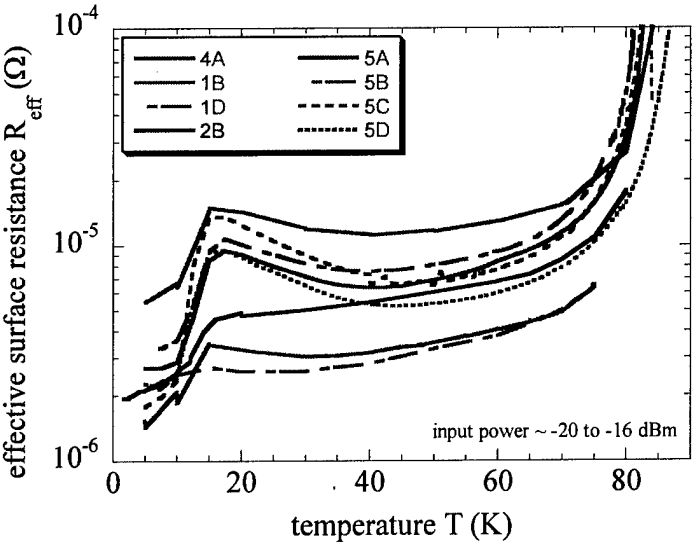

Figure 2. Temperature dependence of the total microwave losses for YBCO films on MgO from four different batches. Batches #1 and #2 were cooled after film deposition at a cooling rate of 10 °C/min, batches #4 and #5 at the much slower cooling rate of 5 °C/min. The slow cooling enhances the dielectric losses of MgO.

The data in table I and Fig. 3 contain no indication of the beneficial effects from Ca-doping, which rather were observed in granular YBCO films [13,18]. Vice versa, the #5-films are concluded to have very few large-angle grain boundaries, if any, and oxygenation levels well in the overdoped region. Both conclusions are confirmed by Fig. 4, which displays the I_{RF}-dependence of the surface resistance and changes of the surface reactance for sample #5A in comparison with the three films of batch #3, for T = 50 K (table I and [5]). The range of linear microwave response for #5A is almost twice as large as that for the overdoped film #3D

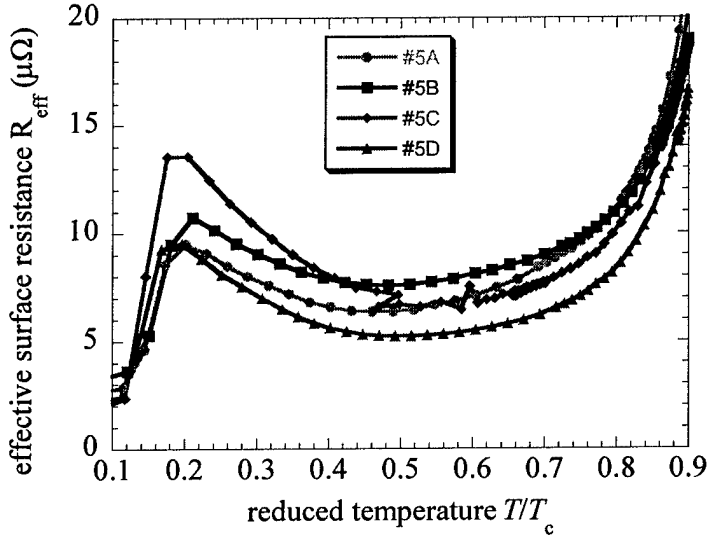

Figure 3. Total microwave losses for the films of batch #5 versus reduced temperature.

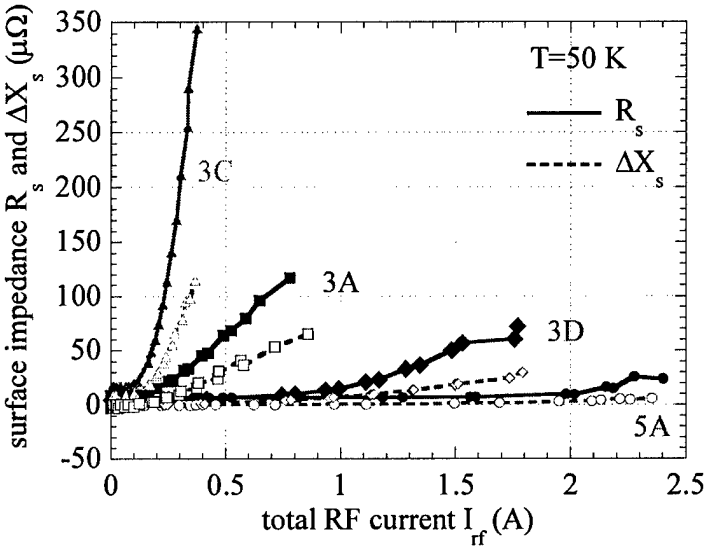

Figure 4. RF-current-dependence of the surface resistance (solid curves, filled symbols) and changes of the surface reactance (dashed curves, open symbols) for four films covering the range of strongly underdoped (#3C) to overdoped (#5A). The current-dependence of the surface resistance is stronger than that of the surface reactance in all cases. Both types of nonlinearity decrease with increasing oxygenation level.

(see also comparative data in Sec. 3.2), yielding a critical RF current of $I_{c,RF} \sim 2$ A. This value corresponds to a magnetic flux density of $B_{RF} \sim 60$ mT, which comes close to the lower critical field expected for bulk single-crystalline YBCO for in-plane shielding currents. The linear range is expected to be limited at this field level by vortex nucleation and motion [1]. For the given resonator geometry, with a resonant volume of ~ 0.003 cm^{-3}, the power circulating in the resonator at $I_{c,RF} \sim 2$ A amounts to $P_{circ} \sim 170$ W. If this value were compared with a disk resonator at the same frequency, which occupies a volume larger by about a factor of 210, the scaled value of P_{circ} would be 36 kW. Finally, accounting for an approximately fivefold enhancement of the RF current at the edges of the stripline compared to the total current, the circulating power would amount to ~ 1 MW. This numerical example demonstrates the high film quality achieved with batch #5, which comes close to or even exceeds the P_{circ}-values achieved with TM_{010} disk resonators at this temperature [1,19].

We noted earlier [5], that the temperature dependence of the resistive nonlinearity can be scaled by the RF current, independent of the oxygenation level. We expect a similar scaling behaviour for the surface reactance. The critical RF current, therefore, is a major parameter describing the nonlinear surface impedance. Altogether, we observe a systematic and reproducible variation of $I_{c,RF}$, at a given temperature, by a factor of ~ 7 for the investigated range of oxygenation levels from strongly underdoped to highly overdoped (c.f., Fig. 7).

Fig. 4 also shows that the resistive nonlinearity is stronger than the reactive, i.e., induc-

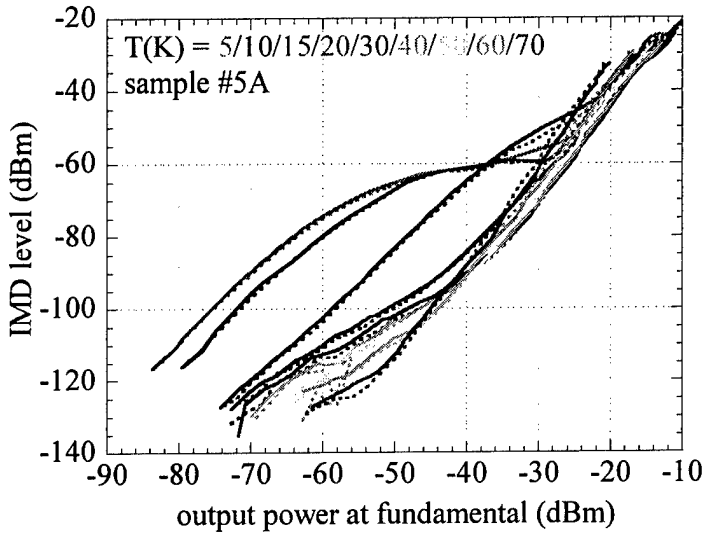

Figure 5. Evolution of the IMD-signal with temperature for sample #5A. The enhanced IMD due to the nonlinear dielectric loss tangent of MgO disappears at elevated temperature. The power dependence of this evolution is depicted in greater detail in Fig. 13.

tive, nonlinearity in our high-quality YBCO films on MgO. This is an important experimental fact, as numerous groups tend to neglect the resistive contributions to nonlinear effects like intermodulation distortion or harmonic generation, especially in resonant devices (Sec. 3.3).

Fig. 5 illustrates the temperature dependent IMD signal versus output power at the fundamental tones for #5A. The broad plateau below 20 K is associated with the dielectric nonlinearity in MgO [4]. For increasing temperature, the IMD signal decreases continuously at low power, but passes through a minimum at intermediate power levels. Cuts through the diagram at constant power are shown in Fig. 13 below and discussed in further detail there.

Fig. 6 compares the IMD levels of the films introduced in Fig. 4. The data clearly show decreasing IMD for increasing oxygenation level. At intermediate output power, we find a variation of the IMD level among the four samples of ~ 30 dB. According to general arguments and confirmed by our model in Sec. 3.3, a third-order nonlinearity like intermodulation distortion depends quadratically on the quadratic coefficients of $R_s(I_{RF})$ and $\Delta X_s(I_{RF})$. Since the nonlinear surface impedance can be scaled by the current, the IMD signal is expected to depend on the fourth power of $1/I_{c,RF}$. An increase of $I_{c,RF}$ by a factor of 7 corresponds, therefore, to a reduction of the IMD level of ~ 34 dB, which is close to what we observe. This consistency indicates that the two types of nonlinearity, $Z_s(I_{RF})$ and IMD, are caused by a single mechanism, despite the very different time scales involved. We are also led to speculate that the dependence of $I_{c,RF}$ on the oxygenation level bears a clue to the microscopic understanding of the nonlinear microwave response of YBCO.

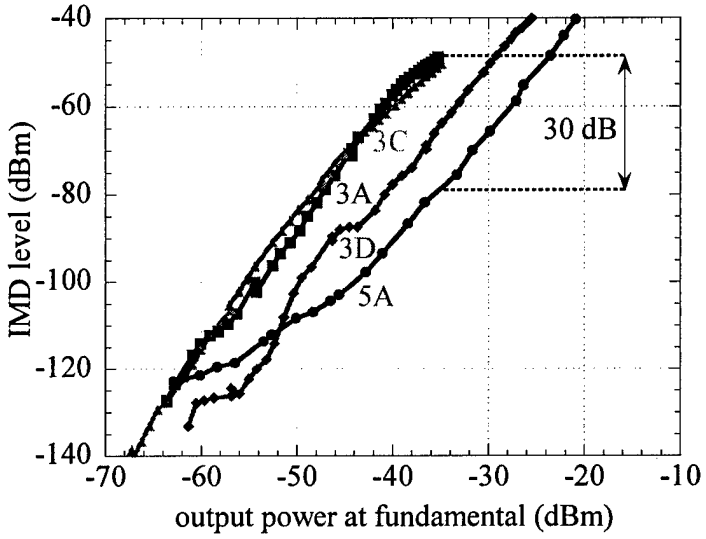

Figure 6. Comparison of the IMD signal versus output power at the fundamental tone for the four films described in Fig. 4, for $T = 50$ K. The intermodulation distortion decreases for increasing oxygenation level.

3.2 Updated correlation plots

The trends for $I_{c,RF}$ and P_{IMD} discussed along with Figs. 4 and 6 are generalized in Figs. 7 and 9, to include all samples studied until now. Fig. 7 displays the correlation between the RF critical current and the DC critical current density for $T = 50$ K. The relationship is almost linear with no sign of saturation. The highest critical currents were achieved with the latest batch, #5. The graph yields a mean slope $\partial I_{c,RF}/\partial J_c \sim 10^{-7}$ cm^2. Interpreting this value as an

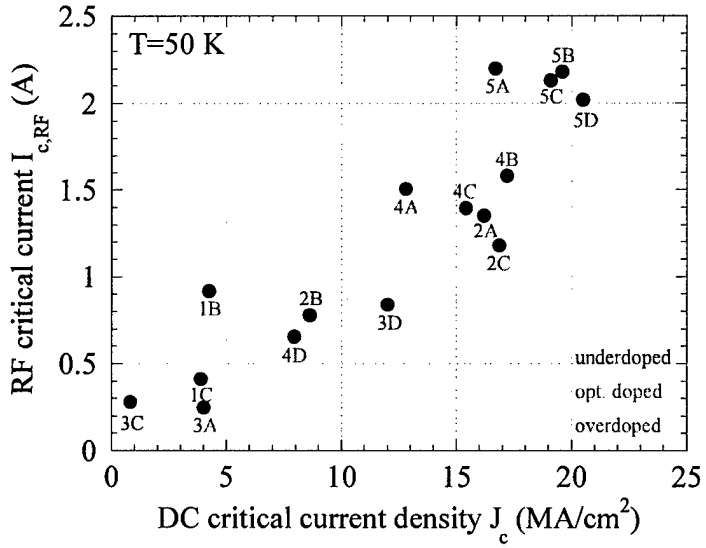

Figure 7. Correlation between the RF critical current and the DC critical current density for $T = 50$ K. $I_{c,RF}$ increases almost linearly with J_c, with a slope ~ 0.1 A/(MA/cm^2). The four films of batch #5 (table I) display the highest critical parameters of all samples studied until now.

effective cross-section of the current path, whose height is approximately limited by the film thickness, $t \sim 350$ nm, we find a range of widths between 20 and 75 μm. If the critical current densities at DC and RF frequencies were equivalent, this length scale would indicate a typical domain size of undisturbed current flow. It is worth noting that this dimension appears consistent with the distribution of the RF current across the width of the stripline (150 μm). RF measurements on different resonator geometries could be used to verify the equivalence of RF and DC critical currents.

According to Fig. 7, the dominant source of the nonlinear microwave response has the same origin as the breakdown of the inductive shielding of low-frequency currents. It has been argued that twin domain boundaries or oxygen vacancies could reduce the critical current density by depinning [20]. This point-of-view would be consistent with the correlation between the DC critical current density and the *c*-axis parameter of epitaxial YBCO, shown in Fig. 8 for some samples. However, the scatter in this and other correlation plots indicates that the electronic properties of the YBCO films are not determined by the oxygen *content* alone, but likely by the *ordering* of the oxygen vacancies, too. This aspect, which could be investigated, e.g., by systematic studies of the orthorhombicity of the films, should be a major focus of research activities following this project.

Fig. 9 displays the linear relation between the third-order intercept (TOI), relative to the output power at the fundamental tones, and the DC critical current density. The overall variation of the TOI is slightly less than the 30 dB expected from the IMD data in Sec. 3.1. This discrepancy can be attributed to deviations of the IMD slope *m* from the exact value 3, as

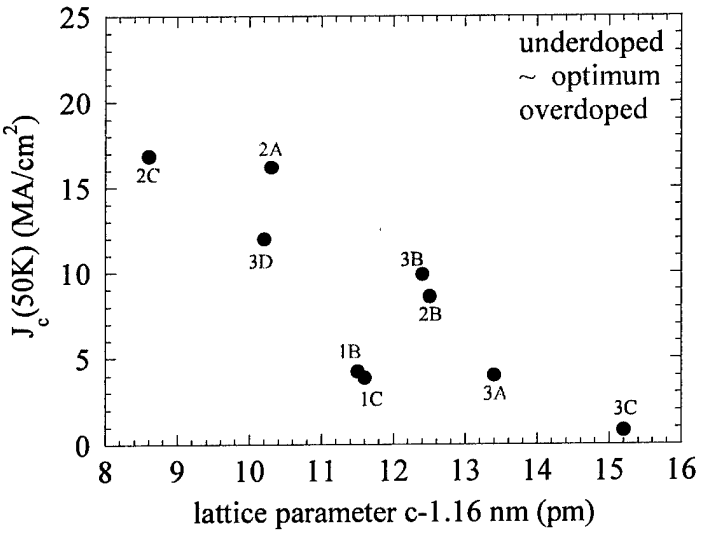

Figure 8. Correlation between the DC critical current density at $T = 50$ K and the c-axis lattice parameter for some films studied in this project (c.f., table I).

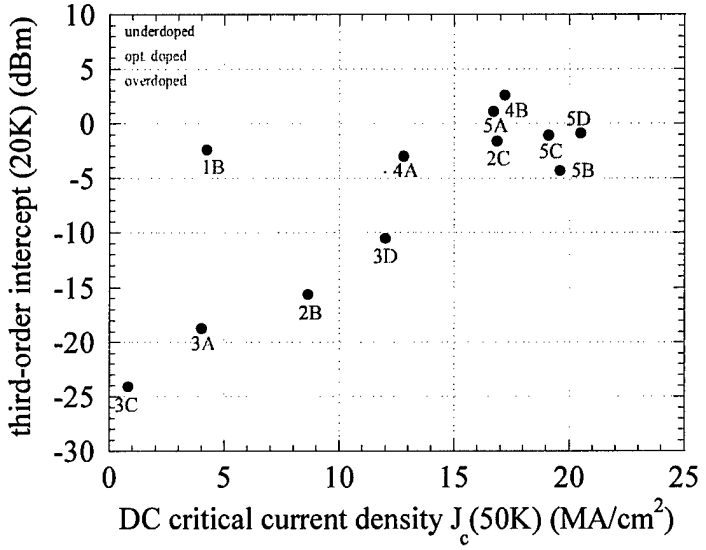

Figure 9. Correlation between the third-order intercept at $T = 20$ K and the DC critical current density at $T = 50$ K. The TOI increases almost linearly with J_c, with a slope ~ 2 dBm/(MA/cm^2). The film #1B falls apart from the overall trend for reasons not yet known.

illustrated by Fig. 10. The slopes observed for the latest batch of films, $m \sim 2.8$, are higher than could be anticipated on the basis of the preceding results [5]. The majority of films now displays slopes between 2.5 and 3. In retrospective, it seems as if the small IMD slopes of #2C and the films of batch #4 could have been due to some kind of defects. At least for batch 4, this assumption is in accordance with the steep inductive nonlinearity at low RF currents [6], which pointed to the presence of weak links that may have been the result of damage introduced during the patterning process.

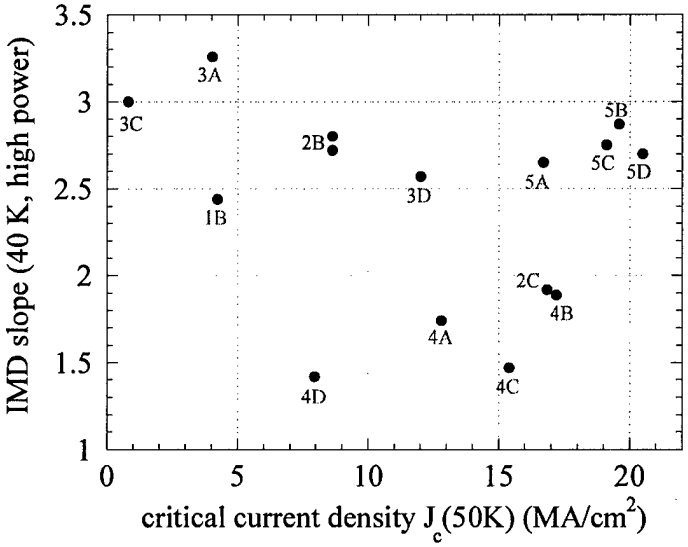

Figure 10. Correlation between the IMD slope at $T = 40$ K and the DC critical current density at $T = 50$ K.

As for the nonlinear surface impedance, we conclude that the intermodulation distortion, too, is determined to a major extent by the critical parameter $I_{c,RF}$, or J_c, respectively.

3.3 IMD model

We have developed a theoretical model to provide a solid base for the analysis of our IMD measurements described above. While other groups have treated similar problems in the literature [16,17,21], our aim was to relate the measurable IMD signal to other, measurable, quantities like the quadratic coefficients of the current-dependent resonant frequency and unloaded quality factor. As a starting point, we have used the equivalent circuit depicted in Fig. 11a. This lumped-element representation was successfully employed for the calculation of the linear current in a resonator for a given input power [22]. We have adapted this model to the nonlinear case as indicated by Fig. 11b. There, V_{IMD} is the voltage generated by the nonlinear inductor and resistor. We have used the following ansatz for the nonlinear circuit elements:

$$X(I_{RF}) = X_0 + X_2 I_{RF}^2, \tag{1}$$

where X stands for the reactance or resistance per unit length, ωL or R. The quadratic coeffi-

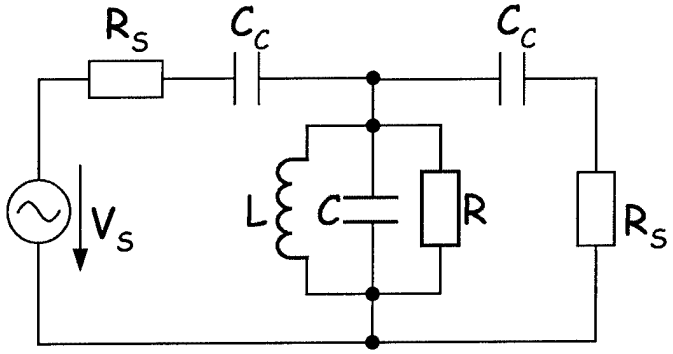

Figure 11a. Equivalent-circuit model of a capacitively coupled resonator (red) terminated by a voltage source at the input and a matched load at the output. This circuit is used for the calculation of the linear current [22].

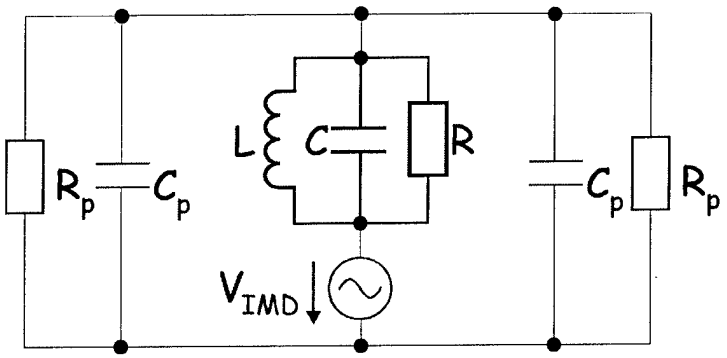

Figure 11b. Equivalent-circuit model used for the calculation of the IMD current [15]. This circuit is based on the all-parallel version of the linear circuit depicted in Fig. 11a. The voltage source contains contributions to the IMD current from both inductor and resistor.

cient X_2 is in units of Ω/A^2m; I is the total current at the two input frequencies (fundamental tones):

$$I = I_0 \cdot (\cos\omega_1 t + \cos\omega_2 t). \tag{2}$$

We have checked the results of our calculation with a separate analysis of a distributed resonator [15], similar to the treatment of Dahm and Scalapino (DS) [16]. The analysis of lumped-element and distributed resonators led to the same expression for the IMD signal P_{IMD}, to within a factor $\pi/3$, which we neglect in the following:

$$P_{IMD} = \left(\frac{12}{\pi^2 Z_0}\right)^2 \cdot \left[r_v(1-r_v)Q_0\right]^4 \cdot P_{in}^3 \cdot \left[\left(\frac{f_2}{f_0}\right)^2 + \left(\frac{Q_2}{2Q_0^2}\right)^2\right] \text{ or} \tag{3a}$$

$$P_{IMD}(dBm) = -91.74 + 40 \cdot \log\left[r_v(1-r_v)Q_0\right] + 3P_{in}(dBm) + 10 \cdot \log\left[\left(\frac{f_2}{f_0}\right)^2 + \left(\frac{Q_2}{2Q_0^2}\right)^2\right], \tag{3b}$$

with Z_0 = 47 Ω the characteristic impedance of the stripline resonator, $r_v = (P_{out}/P_{in})^{1/2}$ the voltage insertion ratio, Q_0 the unloaded quality factor, P_{in} and P_{out} the powers at input and output of the resonator, and f_2 and Q_2 the quadratic coefficients of resonant frequency and unloaded quality factor. The latter are related to X_2 by:

$$\frac{f_2}{f_0} = -\frac{L_2}{2L_0}, \quad \frac{Q_2}{Q_0} \approx -\frac{R_2}{R_0}. \tag{4}$$

The contribution of the inductive nonlinearity to $Q_0 = \omega L/R$ is smaller by a factor $1/Q_0$ than its contribution to f_2 and can hence be neglected.

Eq. (3) contains the expected cubic dependence of P_{IMD} on P_{in}, which is an inherent feature of the model. P_{IMD} depends also on the Q-factor of the resonator, via Q_0 and r_v. If the quality factor itself depends on the input power, the functional dependence $P_{IMD}(P_{in})$ will be modified, and the original behaviour of f_2 and Q_2 can be masked. The result in Eq. (3) resembles the DS-result except for a different prefactor (3/2) that essentially results from a different normalization, and the different weighting of resistive and inductive nonlinearities. We have convinced ourselves that both types of nonlinear contributions are equally important. Ways to access their relative weight by experiment have been proposed in [15,17].

In order to account for the explicit Q-dependence of P_{IMD} in Eq. (3) properly, the equation can be rewritten in terms of the loaded Q-factor and the Q-factor associated with the (symmetric) coupling, Q_{rad}:

$$P_{IMD} = \left(\frac{6Q_{rad}}{\pi^2 Z_0}\right)^2 \cdot Q_L^2 \cdot P_{out}^3 \cdot \left[\left(\frac{f_2}{f_0}\right)^2 + \left(\frac{Q_2}{2Q_0^2}\right)^2\right] \tag{5a}$$

$$P_{IMD} = \left(\frac{6}{\pi^2 Z_0 \sqrt{Q_{rad}}}\right)^2 \cdot Q_L^2 \cdot P_{circ}^3 \cdot \left[\left(\frac{f_2}{f_0}\right)^2 + \left(\frac{Q_2}{2Q_0^2}\right)^2\right] \tag{5b}$$

Eq. (5a) relates the IMD signal to the output power at the fundamental tone, whereas Eq. (5b) refers to the circulating power, $P_{circ} = P_{out}/Q_{rad}$. It is worth noting that the Q-scaling of P_{IMD} involves Q_L^2 in both cases.

We have adapted our model to calculate the IMD signal expected from f_2 and Q_2 for the two films #3D and #5A, with the results summarized in Fig. 12. The quadratic coefficients were extracted from the corresponding RF-current dependences by fitting polynomials of order 2 (quadratic) or 4 (quartic) to the data. We find satisfactory agreement between calculation and measurement at elevated power. We attribute the discrepancy at low power to a weakness related to the determination of the quadratic coefficients, as these cannot be separated properly from the linear background.

For both samples studied in Fig. 12, the resistive nonlinearity was stronger than the inductive contribution to the IMD signal, as summarized in table II. This table also illustrates how sensitive the extracted nonlinear coefficients depend on the way how they are determined. We note that the relative strength of the resistive nonlinearity is smaller for the better film #5A. Further studies should investigate the weighting of the two nonlinear contributions in greater detail, e.g., by phase-sensitive measurements [23].

Type of fit	#3D	#5A
quadratic	6.82	3.18
quartic	33.33	16.45

Table II. Summary of results obtained for the ratio of the normalized quadratic coefficients, $(Q_2/2Q_0^2)/(f_2/f_0)$, deduced from quadratic and quartic fits, respectively, as explained in the text.

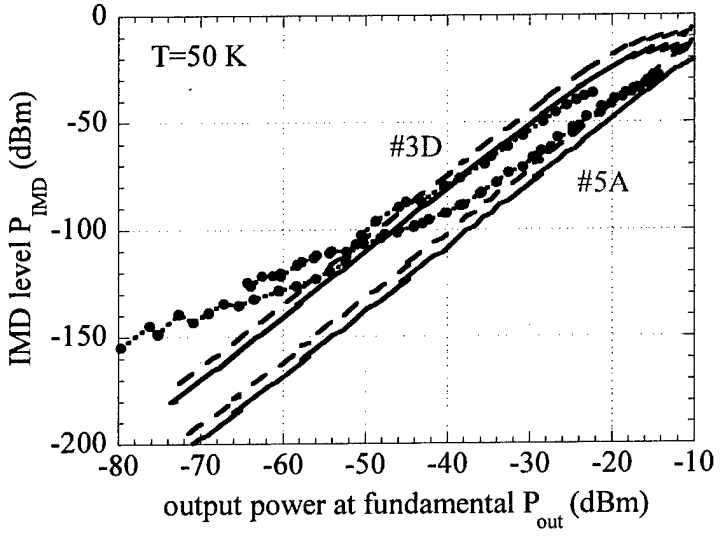

Figure 12. Comparison between the measured IMD signal (symbols) and the calculated results (lines) for samples #3D (blue) and #5A (red) for $T = 50$ K using quadratic (solid lines) and quartic fits (dashed lines). The agreement at elevated power results from a dominant contribution of the resistive nonlinearity (table II).

4. Nonlinear microwave response of MgO

The consequences of resonant absorption in MgO have been analyzed and discussed in detail in previous reports [4-6]. We focus here on new results, which could be identified thanks of the high film quality of batch #5. Fig. 13 displays the temperature dependent microwave losses for #5A for two extreme power levels (dark-blue and light-blue curves, left-hand ordinate). The two most striking features are the minimum of the losses around $T = 40$ K at a relatively high level, $R_{eff} \sim 10$ μΩ, and the splitting into low-power and high-power branches below $T = 20$ K, which is associated with the resonant absorption. We attribute the minimum to the superposition of two counter-acting mechanisms: the decrease of dielectric losses caused by defect dipole relaxation, and the increase of losses in the superconductor as the critical temperature is approached. We have found that the losses due to dielectric relaxation were higher in YBaCuO films that were more slowly cooled from their deposition temperature to ambient (c.f., Fig. 2 and Fig. 14). This is consistent with the nonlinear behaviour of the substrate being due to resonant absorption by $Mg(OH)_2$ impurity states [24].

Fig. 13 also shows temperature dependent IMD-data for constant output power at the fundamental tone (dark-green and light-green solid curves, right-hand ordinate). These data represent "vertical cuts" through the curves of Fig. 5, for two selected values P_{out} = -60 dBm and -40 dBm. Both curves feature a pronounced drop of IMD at the temperature where the resonant absorption in MgO disappears. Interestingly, for the lower output power, the IMD-signal keeps dropping up to the highest temperature, $T \sim 70$ K, while the IMD-level increases

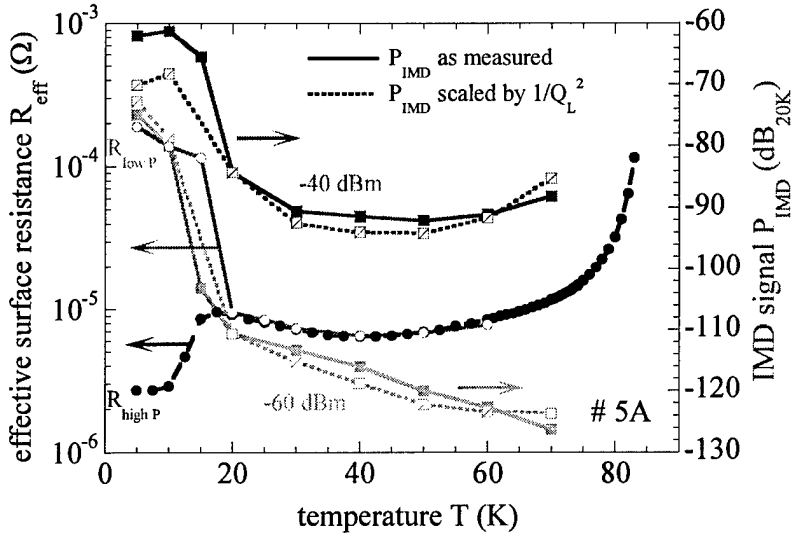

Figure 13. Temperature dependence of R_{eff} (left-hand ordinate) at the lowest measured power (light-blue) and at its minimal value (dark-blue). Displayed on the right-hand ordinate is the IMD signal for two levels of output power (light-green: P_{out} = -60; dark-green: -40 dBm). The dotted curves represent the IMD signal after scaling with respect to the temperature and power-dependent loaded Q-factor [Eq. (5)].

smoothly above about 50 K for the higher output power. This increase is due to the growing influence of the superconducting nonlinearity near T_c. However, at 70 K, the IMD at low and high power still only differ by about four orders of magnitude, not the 60 dB that would be expected from a purely cubic power dependence.

These features of the temperature-dependent IMD could be affected, at least partly, by the power- and temperature-dependent Q-factor [see Eq. (5)]. To check for such ambiguities, we have scaled the measured IMD signal by $[Q_L(20K)/Q_L(T)]^2$, leading to the green dotted curves in Fig. 13. The comparison of solid and dotted curves reveals that the loaded quality factor does affect the measurable IMD signal, and that Q-scaling is necessary. But it shows also that the main features discussed above remain unchanged. This result confirms the enhanced IMD caused by the nonlinear loss tangent of MgO.

In our earlier data, the nonlinearities caused by the superconducting films masked the dielectric nonlinear contributions from the substrate already at temperatures below about 50 K. Our new results, which were obtained for films with a very weak superconducting nonlinearity, reveal that the dielectric losses in MgO persist up to $T = 70$ K. This result needs to be taken into account for most microwave applications of HTS, which are tailored to a temperature region between 50 and 80 K. Unfortunately, using our superconducting stripline technique, we were not able to measure the nonlinear loss tangent and IMD of the MgO alone, which could persist to even higher temperatures. We suggest dielectric resonators to study the nonlinear response of MgO in more detail. We note in passing that the dielectric nonlinearity,

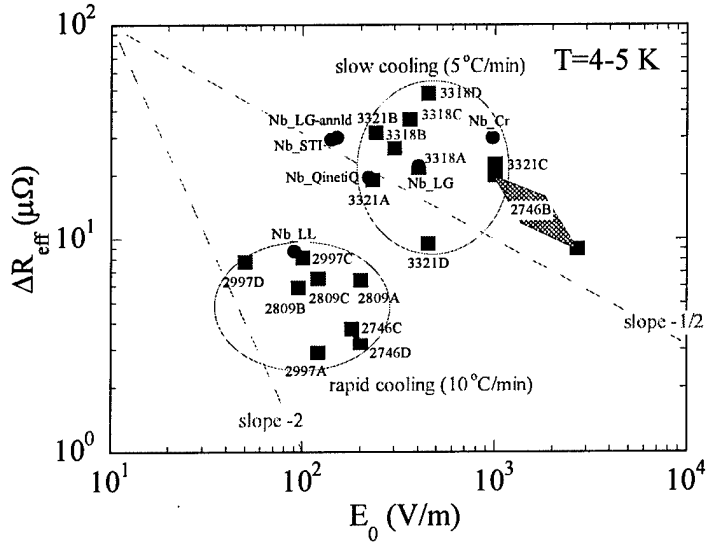

Figure 14. Parametric plot monitoring the dielectric loss tangent and the saturation field of MgO for $T \sim 4$ K. The plot contains data for YBCO films (red colour) as well as for Nb reference films (blue). The effect of slow cooling in terms of enhanced ΔR_{eff} and tendentially increased E_0 is clearly visible. The dashed lines are guides to the eye (c.f., [6]).

which is undesirable for microwave applications of HTS, may be beneficial for RF signal processing with dielectric materials.

Fig. 14 summarizes the parameters describing the nonlinear loss tangent of MgO, for all samples studied in the course of this project. The results for batch #5 added new evidence that slow cooling of the films after deposition are detrimental to the dissipation losses in MgO. According to the data for #4D, the enhanced loss tangent can be reduced, at least partly, by post-deposition annealing. This possibility opens the potential for simultaneous optimization of the oxygenation state of the superconducting films and the loss tangent of the MgO.

5. Open questions, perspectives for future research activities

The aims of the project specified in Sec. 1 could be achieved to a great extent. However, there remain interesting questions to be solved, which could be investigated in future research activities following this project.

5.1 Nonlinearities in the superconductor

1. Study a batch of films rapidly cooled after film deposition, and with the oxygenation state optimized by post-deposition annealing.
2. Study homogeneously Ca-doped films for a set of Ca-concentrations.
3. Investigate the orthorhombicity of the YBCO films used for RF measurements.
4. Perform RF measurements using stripline resonators of different geometry to investigate the correlation between $I_{c,RF}$ and J_c in greater detail.
5. Perform phase-sensitive IMD measurements to judge the relative weighting of resistive and inductive nonlinearities.
6. Investigate the causal relations underlying the microscopic mechanism of the nonlinearities: superconducting order parameter – oxygenation state – J_c – nonlinear microwave response.
7. Refine studies of third-harmonic generation (THG). Our IMD model (Sec. 4) can be used to analyze THG-effects, too. Because the third-harmonic is non-resonant in the stripline resonator due to mode dispersion [10], the magnitude of the measured THG signal depends strongly on the frequency offset between the third overtone and the third harmonic. Since studies of the THG-signal could help distinguish between resistive and inductive nonlinearities, special stripline resonators could be envisaged where both frequencies of interest are resonant.

5.2 MgO-anomalies

8. Study the influence of annealing and quenching, to identify optimal conditions for a low loss-tangent.

9. Perform measurements of the microwave response of bare MgO by, e.g., using a dielectric resonator).

6. Declarations, Acknowledgment, and Disclaimer

6.1 Declaration of Technical Data Conformity

The Principal Investigator of the Contractor, University of Wuppertal, hereby delcares that, to the best of his knowledge and belief, the technical data delivered herewith under Contract No. F61775-01-WE033 is complete, accurate, and complies with all requirements of the contract.

Date: September 24, 2003

Name and Title of Authorized Official: Prof. Dr. Matthias Hein, Principal Investigator

Signature: M. Hein

6.2 Statement relating to Patent Rights

I certify that there were no subject inventions to declare as defined in FAR 52.227-13, during the performance of this contract.

Date: September 24, 2003

Name and Title of Authorized Official: Prof. Dr. Matthias Hein, Principal Investigator

Signature: M. Hein

6.3 Acknowledgment of support and disclaimer

(a) This material is based upon work supported by the European Office of Aerospace Research and Development, Air Force Office of Scientific Research, Air Force Research Laboratory, under Contract No. F61775-01-WE033

(b) Any opinions, findings and conclusions or recommendations expressed in this material are those of the author(s) and do not necessarily reflect the views of the European Office of Aerospace Research and Development, Air Force Office of Scientific Research, Air Force Research Laboratory.

7. References

[1] M.A. Hein, *High-temperature superconductor thin films at microwave frequencies*, Springer Tracts of Modern Physics, vol. 155, Springer, 1999.

[2] M.A. Hein, D.E. Oates, P.J. Hirst, R.G. Humphreys, and A.V. Velichko, "Nonlinear dielectric losses in MgO substrates", *Appl. Phys. Lett.*, **80**, 1007 (2002).

[3] M.A. Hein, R.G. Humphreys, P.J. Hirst, S.H. Park, and D.E. Oates, Contribution to the 7th Symposium on High-Temperature Superconductors, Jonsson Conference Center, Woods Hole, Cape Cod, MA, June 9-12, 2002; to be published in J. Supercond. (2003); cond-mat/0208285.

[4] M.A. Hein, first report for project F61775-01-WE033, February 2002.

[5] M.A. Hein, second report for project F61775-01-WE033, August 2002.

[6] M.A. Hein, third report for project F61775-01-WE033, February 2003.

[7] M.A. Hein, P.J. Hirst, R.G. Humphreys, S.H. Park, D. Seron, and D.E. Oates, Contribution to the European Microwave Conference, EuMC, 7.-9. October 2003, Munich, Germany.

[8] D. Seron, D.E. Oates, A.C. Anderson, J. Mannhart, G. Hammerl, P. J. Hirst, R.G. Humphreys, M.A. Hein, 6th Europ. Conf. on Appl. Supercond. EUCAS, 14.-18. September 2003, Sorrento-Napoli, Italy.

[9] D.E. Oates, S.H. Park, D. Seron, P.J. Hirst, R.G. Humphreys, and M.A. Hein, 6th Europ. Conf. on Appl. Supercond. EUCAS, 14.-18. September 2003, Sorrento-Napoli, Italy.

[10] D.E.Oates, S.-H. Park, M.A. Hein, P.J. Hirst and R.G. Humphreys, Applied Superconductivity Conference 2002, Houston TX, USA, IEEE Trans. Appl. Supercond. **13**, 311 (2003).

[11] M.A. Hein, M. Getta, B. Mönter, S. Kreiskott, P.J. Hirst, R.G. Humphreys, H.N. Lee, S.H. Moon, D.E. Oates, 5th Europ. Conf. on Appl. Supercond. EUCAS, Kopenhagen 2001, Physica C **372-376**, 577 (2002); cond-mat/0111400.

[12] D.E. Oates, M.A. Hein, P.J. Hirst, R.G. Humphreys, G. Koren and E. Polturak, 5th Europ. Conf. on Appl. Supercond. EUCAS, Kopenhagen 2001, Physica C **372-376**, 462 (2002).

[13] G. Hammerl et al., *Nature* **407**, 162 (2000).

[14] H. Obara, A. Sawa, H. Yamasaki, and S. Kosaka, *Appl. Phys. Lett.* **78**, 646 (2001).

[15] D.E. Oates, R.G. Humphreys, and M.A. Hein, to be published.

[16] T. Dahm and D.J. Scalapino, Phys. Rev. **B60**, 13125 (1999).

[17] C. Collado, J. Mateu, and J.M. O'Callaghan, to appear in IEEE Trans. Appl. Supercond. (2003).

[18] H. Obara et al., Appl. Phys. Lett. 78, 646 (2001); Physica C 378-381, 1419 (2002).

[19] H.J. Chaloupka, In "Microwave Superconductivity", H. Weinstock and M. Nisenoff eds., NATO Science Series, Series E: Applied Sciences – Vol. 375, p. 21-53, Kluwer Academic Publishers (2001).

[20] J. Halbritter: Forth EuroCeramics, A. Barone, D. Fiorani, and A. Tampieri eds., Volume 7: High Tc Superconductors, part II, 267 (2000).

[21] E.A. Vopilkin, A.E. Parafin, and A.N. Ruznik, Technical Physics **45**, 214 (2000).

[22] D.E. Oates, A.C. Anderson, and P.M. Mankiewisch, J. Supercond. **3**, 251 (1990)

[23] J.C Booth, S.A. Schima, K. Leong, and D.A. Rudman, 6th Europ. Conf. on Appl. Supercond. EUCAS, 14.-18. September 2003, Sorrento-Napoli, Italy.

[24] B. Henderson and W.A. Sibley, J. Chem. Phys. **55**, 1276 (1971).